

**WL-TR-97-3017**

**STRUCTURAL INTEGRITY ANALYSIS  
AND VERIFICATION FOR AIRCRAFT  
STRUCTURES: VOLUME 2: EFFECTS  
OF COMPRESSIVE LOADING ON THE  
FATIGUE CRACK GROWTH RATES OF  
7075-T651 AND 2024-T3 ALUMINUM ALLOYS**



K.L. Boyd, J.H. Elsner, D.A. Jansen  
Analytical Services & Materials, Inc.  
107 Research Drive  
Hampton, Virginia 23666

J.A. Harter  
WL/FIBEC  
2790 D Street, Room 504  
Wright-Patterson AFB, OH 45433-7402

Final Report for Period 01 Jan - 31 Dec 1995  
August 1996

Approved for public release; distribution is unlimited

FLIGHT DYNAMICS DIRECTORATE  
WRIGHT LABORATORY  
AIR FORCE MATERIEL COMMAND  
WRIGHT-PATTERSON AFB, OHIO 45433-7562

**DTIC QUALITY INSPECTED 3**


**19970804 051**

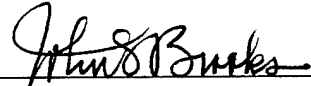
## NOTICE


When Government drawings, specifications, or other data are used for any purpose other than in connection with a definitely Government-related procurement, the United States Government incurs no responsibility or any obligation whatsoever. The fact that the government may have formulated or in any way supplied the said drawings, specifications, or other data, is not to be regarded by implication, or otherwise in any manner construed, as licensing the holder, or any other person or corporation; or as conveying any rights or permission to manufacture, use, or sell any patented invention that may in any way be related thereto.

This report is releasable to the National Technical Information Service (NTIS). At NTIS, it will be available to the general public, including foreign nations.

This technical report has been reviewed and is approved for publication.

  
\_\_\_\_\_  
DAVID S. CONLEY, Structural Integrity Engr  
Structural Integrity Branch

  
\_\_\_\_\_  
JOHN S. BROOKS, Team Leader  
Structural Integrity Branch

  
\_\_\_\_\_  
JOHN ACH, Chief  
Structural Integrity Branch  
Structures Division

If your address has changed, if you wish to be removed from our mailing list, or if the addressee is no longer employed by your organization, please notify WL/FIBE, Building 65, 2790 D Street, Suite 1, Room 504, Wright-Patterson AFB, OH 45433-7402 to help us maintain a current mailing list.

Copies of this report should not be returned unless return is required by security considerations, contractual obligations, or notice on a specific document.

REPORT DOCUMENTATION PAGE			Form Approved OMB No. 0704-0188	
Public reporting burden for this collection of information is estimated to average 1 hour per response, including the time for reviewing instructions, searching existing data sources, gathering and maintaining the data needed, and completing and reviewing the collection of information. Send comments regarding this burden estimate or any other aspect of this collection of information, including suggestions for reducing this burden, to Washington Headquarters Services, Directorate for Information Operations and Reports, 1215 Jefferson Davis Highway, Suite 1204, Arlington, VA 22202-4302, and to the Office of Management and Budget, Paperwork Reduction Project (0704-0188), Washington, DC 20503.				
1. AGENCY USE ONLY (Leave blank)		2. REPORT DATE Aug 96		3. REPORT TYPE AND DATES COVERED Final Report 1 Jan 95- 31 Dec 95
4. TITLE AND SUBTITLE Structural Integrity Analysis And Verification For Aircraft Structures: Volume 2: Effects Of Compressive Loading On The Fatigue Crack Growth Rates Of 7075-T651 And 2024-T3 Aluminum Alloys			5. FUNDING NUMBERS Contract #F33615-94-D-3212 PE: 62201F PR: 2401 TA: LE WU: 01	
6. AUTHOR(S) K.L. Boyd, J.H. Elsner, D.A. Jansen.  J.A. Harter- Wright Patterson AFB				
7. PERFORMING ORGANIZATION NAME(S) AND ADDRESS(ES) Analytical Services and Materials, Inc. 107 Research Drive Hampton, Virginia 23666			8. PERFORMING ORGANIZATION REPORT NUMBER	
9. SPONSORING/MONITORING AGENCY NAME(S) AND ADDRESS(ES) Flight Dynamcis Directorate Wright Laboratory Air Force Materiel Command Wright-Patterson AFB, OH 45433-7562 POC: Lt David Conley, WL/FIBE, (937)255-6104			10. SPONSORING/MONITORING AGENCY REPORT NUMBER  WL-TR-97-3017	
11. SUPPLEMENTARY NOTES				
12a. DISTRIBUTION AVAILABILITY STATEMENT Approved for Public Release; Distribution is unlimited			12b. DISTRIBUTION CODE	
13. ABSTRACT (Maximum 200 words) The purpose of this research was to determine the effects of constant amplitude high compressive stresses on the fatigue life of 7075-T651 and 2024-T3 aluminum alloys. This project consisted of three components: finite element modeling/analysis, generation of fatigue crack growth data for AFGROW modifications, and verification testing. An elastic-plastic finite element analysis program (ZIP2D) was used to determine the stress field in the crack plane for the different testing conditions. Fatigue crack growth data from center-notched, through-cracked panels were collected for both alloys at several loads and stress ratios, and these data were used to modify tabular crack growth data for the AGROW program. Center-notched and surface-cracked specimens were then tested to verify AFGROW predictions (with updated tabular data) for crack shape and fatigue lifetimes.				
14. SUBJECT TERMS Compress Stresses, Fatigue Life, Aluminum Alloys, Fatigue Crack Growth Data, AFGROW, ZIP2D			15. NUMBER OF PAGES 44	
			16. PRICE CODE	
17. SECURITY CLASSIFICATION OF REPORT Unclassified	18. SECURITY CLASSIFICATION OF THIS PAGE Unclassified	19. SECURITY CLASSIFICATION OF ABSTRACT Unclassified	20. LIMITATION OF ABSTRACT SAR	

## TABLE OF CONTENTS

LIST OF FIGURES .....	iv
LIST OF TABLES .....	v
FOREWORD.....	vi
1. EXECUTIVE SUMMARY .....	1
2. INTRODUCTION.....	3
3. FINITE ELEMENT ANALYSIS.....	5
3.1. Finite Element Model .....	6
3.2. Finite Element Results.....	13
4. VERIFICATION TESTING.....	19
4.1. Center-Cracked Panel Testing .....	20
4.1.1. 7075-T651 Aluminum Specimens.....	21
4.1.2. 2024-T3 Aluminum Specimens .....	26
4.2. Surface-Cracked Panel Testing.....	29
4.2.1. 7075-T651 Aluminum Specimens.....	30
4.2.2. 2024-T3 Aluminum Specimens .....	33
4.2.3. Additional Testing.....	33
5. REFERENCES.....	36
APPENDIX A .....	39
Figure A.1: Detailed Information for Specimen Tests.....	39

## LIST OF FIGURES

Figure 1. M (T) Specimen Geometry .....	7
Figure 2. Mesh Detail in the Crack Region .....	8
Figure 3. Finite Element Model .....	9
Figure 4. 2024 Al Stress-Strain Curve.....	10
Figure 5. 7075 Al Stress-Strain Curve.....	10
Figure 6. Load History for R= -6.0 .....	12
Figure 7. Residual Stresses in Crack Plane for 0.5 Inch Crack (2024).....	13
Figure 8. Residual Stresses in Crack Plane for 1.0 Inch-Crack (2024).....	14
Figure 9. Residual Stresses in Crack Plane for 0.5-Inch Crack (7075).....	15
Figure 10. Residual Stresses in Crack Plane for 1.0-Inch Crack (7075).....	16
Figure 11. Composite Fatigue Crack Growth Rate Plot for 7075-T651 Aluminum .....	21
Figure 12. Crack Growth Rate Plot for 7075-T651 Al with $P_{max}$ = 5 kips; R= -0.5 .....	22
Figure 13. Crack Growth Rate Plot for 7075-T651 Al with $P_{max}$ = 5 kips; R= -6.....	23
Figure 14. Crack Growth Rate Plot for 7075-T651 Al with $P_{max}$ = 5 kips; R= -9 .....	23
Figure 15. Composite Data Compared to High and Low Humidity Data for 7075-T651 .....	25
Figure 16. Composite Fatigue Crack Growth Rate Plot for 2024-T3 Aluminum .....	26
Figure 17. Crack Growth Rate Plot for 2024-T3 Al with $P_{max}$ = 5 kips; R= -0.5 .....	27
Figure 18. Crack Growth Rate Plot for 2024-T3 Al with $P_{max}$ = 5 kips; R= -6.....	27
Figure 19. Crack Growth Rate Plot for 7075-T651 Al with $P_{max}$ = 22.5 kips; R= -2.....	34
Figure 20. Crack Growth Rate Plot of 7075-T651 Al with $P_{max}$ = 30 kips; R= -1.5 .....	35

## LIST OF TABLES

Table 1. Load Cases Modeled with ZIP2D .....	11
Table 2. Test Matrix for 7075-T651 & 2024-T3 Al Alloys.....	20
Table 3. Average Crack Growth Rates (in/cycle) at Several $\Delta K$ Levels .....	22
Table 4. Fatigue Lifetimes for 7075-T651 Al Under Reported Testing Conditions.....	24
Table 5. Fatigue Lifetimes for 2024-T3 Al Under Reported Testing Conditions.....	28
Table 6. Fatigue and Crack Shape Data from Precracking to Break-Through .....	30
Table 7. Fatigue Data from Break-Through to Failure for Different Initial Crack Lengths .....	31

## **FOREWORD**

This report was prepared by Analytical Services & Materials, Inc., Hampton Virginia for WL/FIBEC, Wright-Patterson Air Force Base, Ohio, under contract F33615-94-D-3212, "Structural Integrity Analysis and Verification for Aircraft Structures." The contract monitor and government project engineer was Mr. James A. Harter, WL/FIBEC. The period of performance for this report was January 1 to December 31, 1995.

The work for this project (Delivery Order 0002) was performed by Analytical Services & Materials, Inc. personnel, located at the WL/FIBEC Fatigue & Fracture Test Facility, Bldg. 65, Area B, Wright-Patterson AFB, OH. The Principal Investigator of this research was Mr. Kevin L. Boyd. The authors of this report were Mr. Kevin L. Boyd and Mr. John H. Elsner. Technical inputs were submitted by Mr. James A. Harter and Mr. Daniel A. Jansen.

## 1. EXECUTIVE SUMMARY

The purpose of this research was to determine the effects of constant amplitude high compressive stresses on the fatigue life 7075-T651 and 2024-T3 aluminum alloys.

This project consisted of three components: finite element modeling/analysis, generation of fatigue crack growth data for AFGROW modifications, and verification testing. An elastic-plastic finite element analysis program (ZIP2D) was used to determine the stress field in the crack plane for the different testing conditions. Fatigue crack growth data from center-notched, through-cracked panels were collected for both alloys at several loads and stress ratios, and these data were used to modify tabular crack growth data for the AFGROW program. Center-notched and surface-cracked specimens were then tested to verify AFGROW predictions (with updated tabular data) for crack shape and fatigue lifetimes.

The finite element model results did not show that there was any significant difference between the residual stresses in the crack growth plane between the different compressive loading cases for each of the two materials of interest. However, as expected, there was a difference in the residual stresses in the crack growth plane between the 2024-T3 and 7075-T6 aluminum materials.

The experimental data showed that there was a difference in the fatigue crack growth rates in the high ( $R = -6.0$  &  $-9.0$ ) compressive loading cases. This higher compressive loading



resulted in slower crack growth rates, as opposed to the moderate compressive loading case ( $R = -2.5$ ). This data does not show an “acceleration” effect, due to compressive loading in the 2024-T3 material, as reported in earlier studies. In addition, no significant “compressive” effect was observed in the 7075-T6 material. However, due to the limited number of specimens used in this study, it is not clear whether the difference in results between the testing and analysis is due to data scatter, localized crack-face buckling, or other factors.

## 2. INTRODUCTION

The purpose of this research is to determine the effects of compressive loading on the fatigue crack growth rates of 7075-T651 and 2024-T3 aluminum alloys. The data generated in this research will be used to enhance the capabilities of the AFGROW fatigue crack growth life prediction program [1]. Empirical relationships have been developed to predict fatigue crack growth rates as a function of the stress intensity factor ( $K$ ), and the stress ratio,  $R$  (min. stress/max. stress) [2,3]. The stress intensity factor, by definition, does not have meaning under compressive loading, so most current LEFM-based fatigue crack growth life prediction methods do not use negative stress intensity ( $K$ ) values to determine the fatigue crack growth rates. The common practice for accounting for “negative” stress intensity factors is to replace  $\Delta K$  with  $K_{\max}$ , when  $R < 0$ . While negative stress ratios have been shown to have little influence on 7075 aluminum [4,5], they have been shown to affect the crack growth rates of 2024, particularly near threshold,  $K_{th}$ , values [6]. Plasticity-induced, fatigue crack closure has been suggested to be the reason [7].

In the AFGROW code, the assumption made is that for  $R < R_{Lo}$  there is no further effect on  $da/dN$  vs.  $K_{\max}$ . (Typically,  $R_{Lo}$  is in the range of  $-0.4 \leq R_{Lo} \leq -0.2$ ). However, since  $R_{Lo}$  is a subjectively assigned value, it is often a matter of debate within the fracture mechanics community. Therefore, verification testing of specimens subjected to tensile-compressive

constant amplitude fatigue cycles was performed to determine the effect(s) of high compressive stresses on fatigue crack growth rates of 2024 and 7075 aluminum alloys.

### 3. FINITE ELEMENT ANALYSIS

Finite element models were generated for the middle tension (M(t)) specimen geometry, tested in this program. The purpose of the finite element analyses was to examine the residual stress fields in the crack planes, under the actual loading conditions. Specifically of interest are the residual stresses in the direction of specimen loading,  $\sigma_y$ . With the knowledge of these residual "closure" stresses, more accurate insight could be made between the life predictions and actual test results.

The finite element code used to evaluate the elastic-plastic and stress history effects due to the constant amplitude fatigue loading examined under this study, was ZIP2D [8]. ZIP2D is a two-dimensional, elastic-plastic finite element code that uses constant-strain triangular elements and an 'initial stress' approach [9] to approximate nonlinear material behavior. The ZIP2D code also uses incremental loading in order to satisfy both the yield condition (von Mises) and flow rule (Prandtl-Reuss or Drucker) associated with incremental plasticity.

Crack extension and intermittent contact of the crack surfaces are accounted for in ZIP2D by an efficient modification of the structural stiffness matrix. This procedure has the advantage that the complete stiffness matrix does not have to be reformulated and decomposed each time that the crack is extended, closed or opened. Further details can be found in Reference 8. The fatigue loading situations examined in this study were constant

amplitude for several different stress ratios. The ZIP2D code has been used successfully in several studies investigating the effects of fatigue crack closure, fracture criterion for widespread cracking, and fracture analysis of stiffened panels with widespread cracking [10,11,12].

### **3.1. Finite Element Model**

The middle tension specimen geometry modeled in this study is shown in Figure 1. Due to specimen geometry and loading, symmetry was used in which one-quarter of the specimen was modeled. The one-quarter specimen geometry dimensions were 8.0-inches long x 2.0-inches wide x 0.25-inches thick. Two different crack geometries, with half-crack lengths ( $c$ ) of 0.5 inches and 1.0 inches, were analyzed in this study.

To perform the elastic-plastic analysis of these two geometries, 90% of the crack length of interest was modeled, initially, as a “free” surface. Subsequently, the crack was allowed to propagate, under cyclic loading, to its final crack length of interest. This was done for two reasons: first, the model would reflect the stress history effects seen in the crack plane; and second, modeling 90% of the final crack length as a free surface would reduce the model computation time.

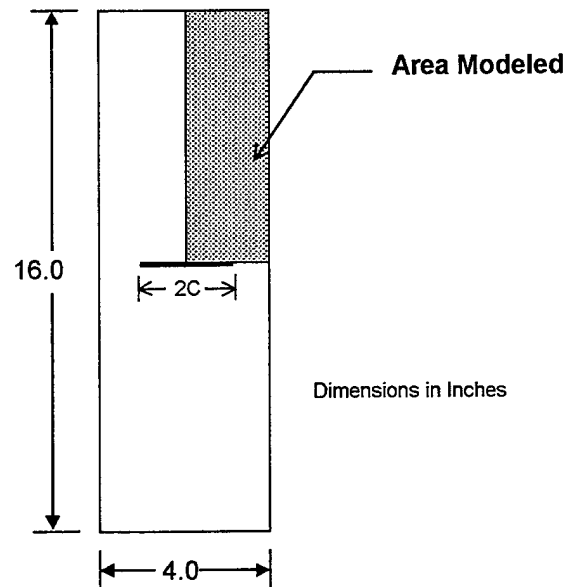


**Figure 1.** M (T) Specimen Geometry

Great care was taken to model the finite element mesh in the region of the crack-tip and crack-propagation direction to ensure accuracy. Element sizes of 0.005 inch were used in the region of the crack tip and direction of crack propagation. This level of detail is shown in Figure 2.

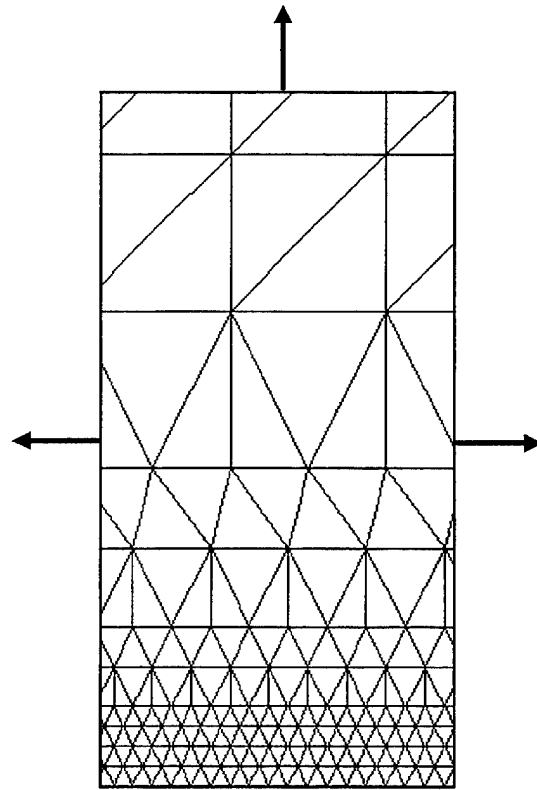


**Figure 2. Mesh Detail in the Crack Region**

Element sizes were conservatively increased away from the crack-tip region. A representation of the whole finite element model can be seen in Figure 3. This meshing procedure was found to be reasonable and compared well to studies previously reported [10,13,14].

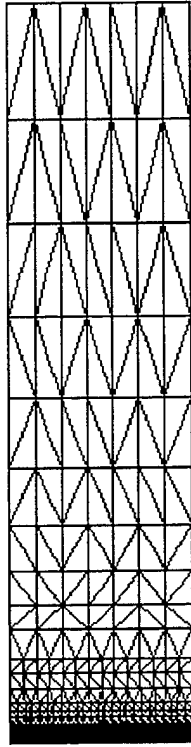


**Figure 3. Finite Element Model**

The material model for the constant-strain triangular elements was piece-wise linear (w/ isotropic hardening) and consisted of six segments. The stress-strain curves for the 2024-T3 and 7075-T6 aluminum materials were approximated from MIL-HDBK-5F Data. These material data curves are shown in Figures 4 and 5. The boundary conditions were symmetric, except in the crack plane, where they consisted of linear springs. For free nodes, the spring stiffness is set to zero. For fixed nodes, the spring stiffness is set to an extremely large (approximately  $10\text{E}+07$  times the modulus of elasticity in the structure) numerical value.



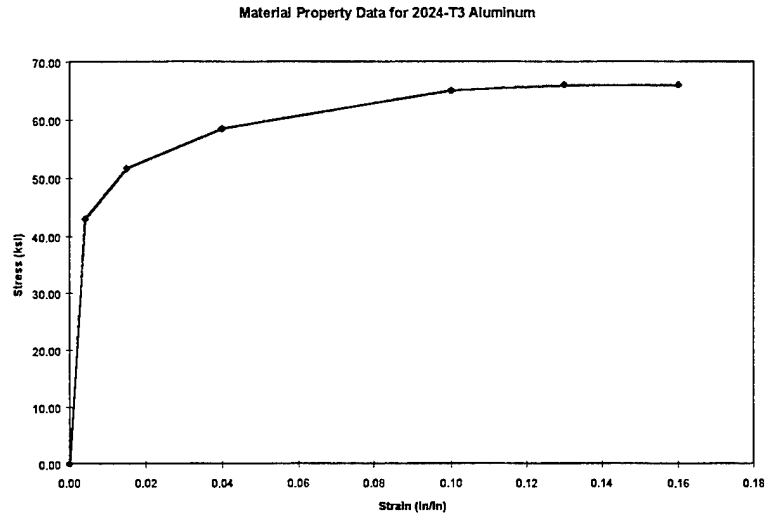


**Figure 4. 2024 Al Stress-Strain Curve**

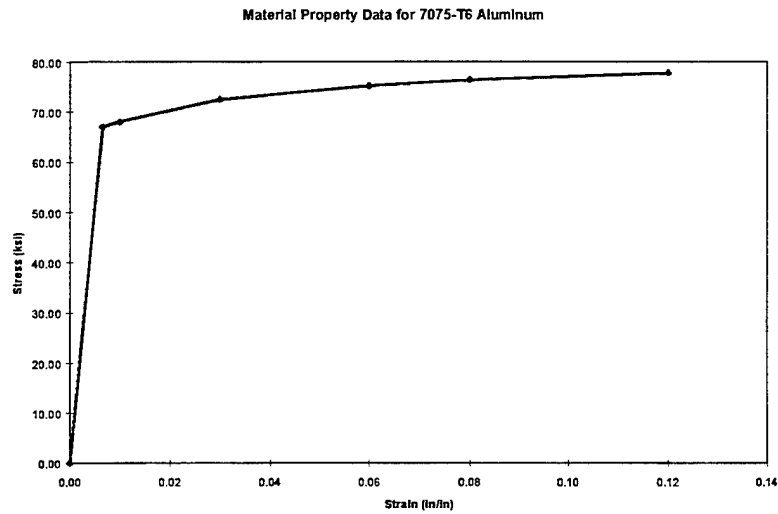


**Figure 5. 7075 Al Stress-Strain Curve**

There was no attempt to incorporate a failure criteria for crack growth. Crack growth was simulated by releasing one node, during each cycle, at the maximum applied stress. This is accomplished by releasing the springs of nodes, upon reaching the maximum opening load (stress) in this study. Therefore, the results of this study should only be viewed as trends in

crack growth behavior. In addition, due to the length of the cracks modeled in this study (0.5 and 1.0 inch), it is possible that stable tearing is already occurring in this region.

The different load cases that were examined in this study can be found in Table 1. The initial test matrix called out for testing at maximum stress levels of 5 ksi at stress ratios (R) of -0.5, -6.0 and -9.0. However, in the 2024-T3 aluminum, the R= -9.0 value was too close to the compressive yield stress of the material, causing buckling failures.

**Table 1. Load Cases Modeled with ZIP2D**

Material (Aluminum)	Max Stress (ksi)	Stress Ratio, R ( $\sigma_{min}/\sigma_{max}$ )		
		-0.50	-6.00	-9.00
2024-T3	5.00	X	X	
7075-T6	5.00	X	X	X

To stabilize any stress history effects, crack growth was initiated 0.05 inches prior to the crack length of interest (approximately 12 cycles in these cases), allowing stresses in the crack plane to equalize. An example of the load history is shown in Figure 6.

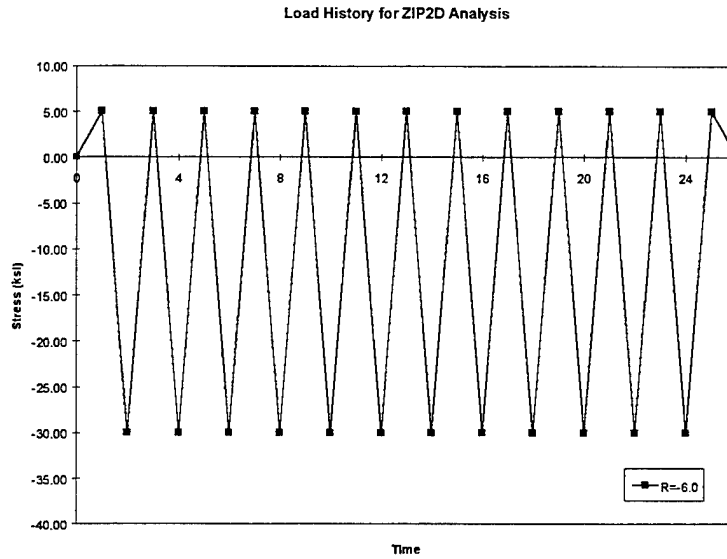


**Figure 6. Load History for R= -6.0**

The ZIP2D code was modified to print out the stresses in the crack plane for maximum, minimum, and approximately zero loading. The tolerances in which the stresses were printed out were within +/- 100 psi of the target load. For the load cases evaluated in this study, the “zero load” values ranged between +/- 70 psi. Therefore, instead of the residual stresses being printed out at exactly 0 psi, they were often some small variation around that value. This small variation had little, or no effect, when comparing the residual stress values between the load cases for the two materials.

### 3.2. Finite Element Results

The results of the elastic-plastic, finite element analysis for the 2024-T3 aluminum showed that there was no difference in residual stresses in the crack plane in the 0.5 inch crack cases for the two stress ratios of interest. The results are shown in Figure 7.

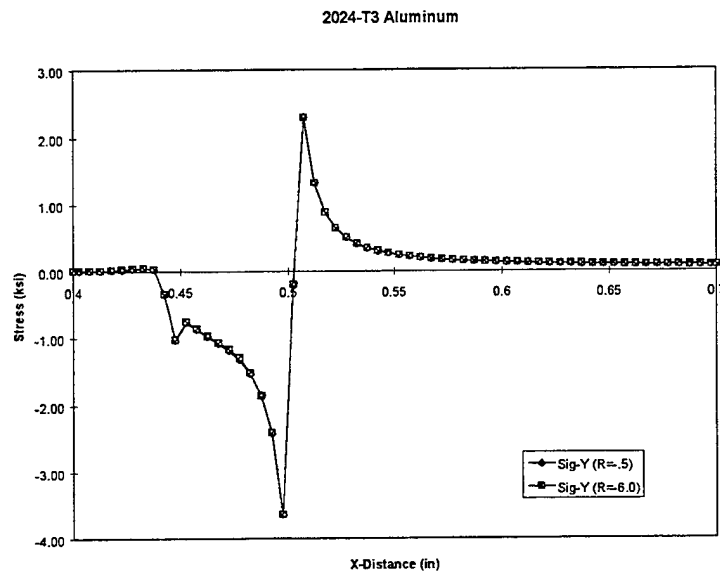
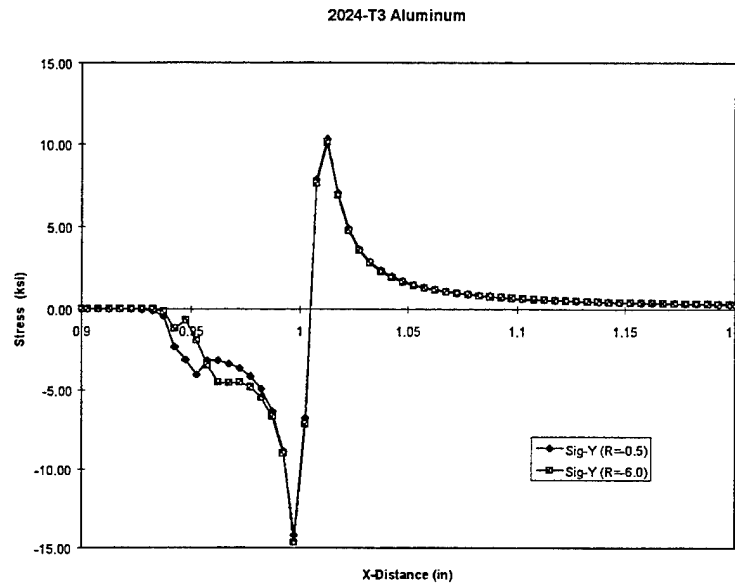


Figure 7. Residual Stresses in Crack Plane for 0.5 Inch Crack (2024)

In the 0.5-inch-crack case, there is a discontinuity in the residual stress distribution behind the crack tip, at an x-distance of 0.45 inch. This point can be attributed to a “build up” of residual stresses, at the point of contact between the “open” and “closed” portions of the crack. This is also the point at which the cyclic loading was initiated, and the first plastic and residual stress zones are coincident. This behavior was present in all load cases, in one form or another.

For the 1.0-inch-long crack case, there appears to be subtle differences in the residual stresses, behind the crack tip. These results are shown in Figure 8.



**Figure 8. Residual Stresses in Crack Plane for 1.0 Inch-Crack (2024)**

This difference is most likely the result of excessive stresses (yielding) experienced in the crack-tip region in the  $R = -6.0$  case. Yielding is also present slightly in front of the crack-tip, at an x-distance of 1.00-1.05 inches. The slight difference in the peak values might also be attributed to the slight difference in the “zero” load stress. The “zero” load stress was approximately 40 psi in one case ( $R = -0.5$ ) and -70 psi ( $R = -6.0$ ) in the other.

Considering the specimen geometry (4.0-inch wide x 0.25-inch thick), a 2-inch (total) crack experiences a net section compressive stress of 60 ksi, well within the plastic range for this material. For the  $R = -0.5$  case, the net section stress would be approximately 5 ksi, or still

within the linear response range of the material. When comparing these two situations, one might expect some differences in the stress profiles overall. However, it should be noted that there should be no significant amount of difference in the crack opening load between these two cases. Therefore, it might be surmised that the crack-growth behavior between these two situations would be very similar, if not, exactly the same.

The results of the elastic-plastic, finite element analysis for the 7075-T6 aluminum showed that there was no difference in residual stresses in the crack plane for the 0.5-inch crack or the 1.0 inch-crack cases. Due to the higher yield strength capabilities of this alloy, there were three stress ratios to compare. The results are shown in Figures 9 and 10.

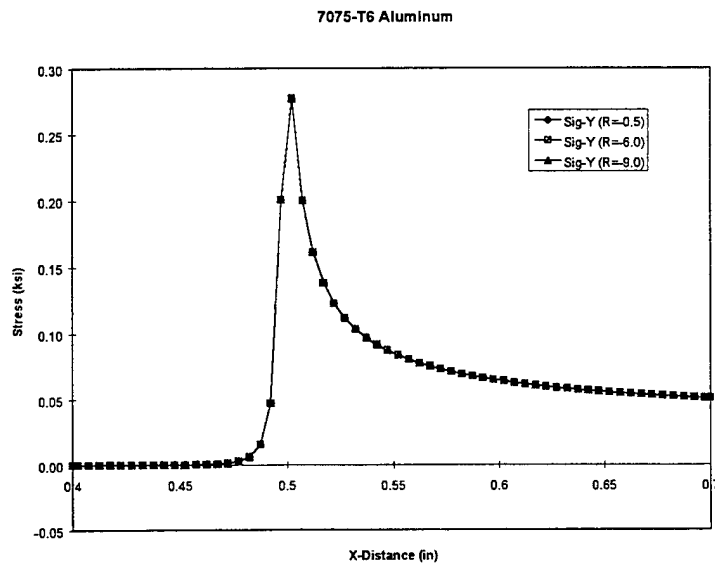


**Figure 9. Residual Stresses in Crack Plane for 0.5-Inch Crack (7075)**

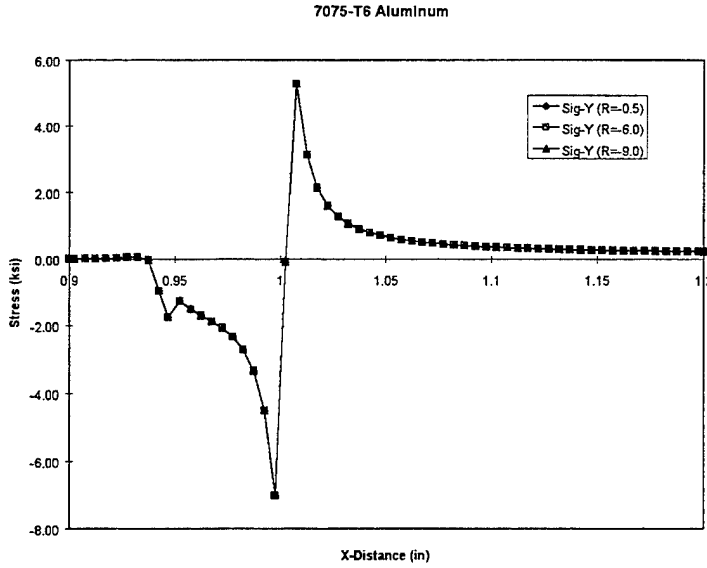


Figure 10. Residual Stresses in Crack Plane for 1.0-Inch Crack (7075)

In Figure 9, it is shown that there are no negative compressive residual stresses in the crack plane. This is not an accurate representation of the stresses in the crack plane for this situation. The reason for this absence of negative stresses is that the finite element model used in this study was not refined enough in the area of the crack tip to properly reflect the residual stresses in the plastic zone for this combination of material, geometry and loading conditions. A quick calculation of an Irwin (circular) plastic zone concludes that the plastic zone radius,  $r_p$ , for this situation is less than 0.002 inch. The Irwin plastic zone can be calculated by the formula:

$$r_p = \frac{1}{2\pi} \left( \frac{K_I}{\sigma_{YS}} \right)^2 \quad (1)$$

where:

$K_I$  = Mode I stress intensity factor  
 $\sigma_{YS}$  = material yield stress

Since the size of the elements in the vicinity of the crack tip were approximately 0.005 inch, it would follow that the finite element analysis would "miss" the displacements (and consequently stresses) within the small plastic zone at the crack tip.

However, after examining the 1-inch-crack case (Figure 10), there appears to be no difference in the residual stresses in the crack plane between the three cases. This would suggest that for the 0.5-inch-crack case (Figure 9), there would also be no difference between the three cases. This is because, for the 0.5-inch-crack case, the stress intensity factors  $K_I$  (and plastic zones) are much smaller, and therefore LEFM (Linear Elastic Fracture Mechanics) criteria would be met more rigorously. It is for these reasons, and increased modeling time, that the 0.5-inch-crack case analysis was not repeated in this study.

In summary, it could be concluded that for the load cases examined, there should be no differences in the fatigue crack growth rate behavior between loading conditions for each material. It should be noted that these conclusions are based only on the residual stress field similarities under similar loading conditions (stress, frequency, wave shape, R). Many other material-related factors influencing the fatigue crack growth rate are: material chemistry, product form, heat treatment, material anisotropy, batch to batch variation in material processing and plate thickness. Several environmental conditions affecting the fatigue crack growth rates could be environment (humidity, salt water, etc.) and temperature. Therefore, in real testing (and service) environments, extreme differences in



crack growth rate behavior could be observed, unless there is a conscious effort made to control these variables.

#### 4. VERIFICATION TESTING

All verification testing was performed in the Fatigue and Fracture Test Facility, Bldg. 65, Area B, WPAFB, OH. Two 100 kip and one 50 kip MTS servo-hydraulic fatigue test frames, using 50% load range settings, were used to test all the specimens. The test frames were operated in load control with MTS 458 test controllers at frequencies of 8-10 Hz. Sinusoidal load control signals were generated with MS-DOS based computers running MATE software.

Center-cracked and surface-cracked panels (3.95 x 16 x 0.25 inches) of 7075-T651 and 2024-T3 aluminum were tested, under constant amplitude loading in laboratory air. Buckling guides were used to prevent specimen buckling under high compressive loading. Crack lengths were monitored by optical methods, and a total of 16 and 5 center-cracked and surface-cracked specimens were tested, respectively. The test matrix is shown in Table 2. A more detailed list, including specimen ID, testing dates and machine usage can be found in the Appendix A.

**Table 2. Test Matrix for 7075-T651 & 2024-T3 Al Alloys**

Alloy	Configuration	Max Load (kips)	R	Number of tests
7075-T651	Center cracked	5.0	-0.5	3
7075-T651	Center cracked	5.0	-6.0	2
7075-T651	Center cracked	5.0	-9.0	4
7075-T651	Center cracked	22.5	-2.0	2
7075-T651	Center cracked	30.0	-1.5	1
2024-T3	Center cracked	5.0	-0.5	2
2024-T3	Center cracked	5.0	-6.0	2
7075-T651	Surface cracked	7.0	-4.0	3
2024-T3	Surface cracked	7.0	-4.0	2

Unless otherwise noted,  $\Delta K$  is taken to be  $K_{\max}$  in this report for all cases, when R is less than zero.

#### **4.1. Center-Cracked Panel Testing**

The center-cracked panels had a 0.20-inch EDM notch machined in the center of the panel. All specimens were precracked, using a load shedding procedure, from 9.9 kips to 5.0 kips in increments of about 1 kip and crack increments of approximately 0.01 inch. This was done in order to reduce the amount of time it would take to generate a suitable maximum stress and crack length for testing. This procedure was also performed in order to remove any “stress history” effects on the crack tips imposed by the previous higher loads. A stress ratio of -0.5 was used for precracking, and testing began at crack length,  $c$ , of at least 0.1-inch past the notch tip.

#### 4.1.1. 7075-T651 Aluminum Specimens

Twelve 7075-T651 aluminum center-cracked specimens were tested. A composite of all the  $da/dN$  vs.  $\Delta K$  data can be seen in Figure 11.

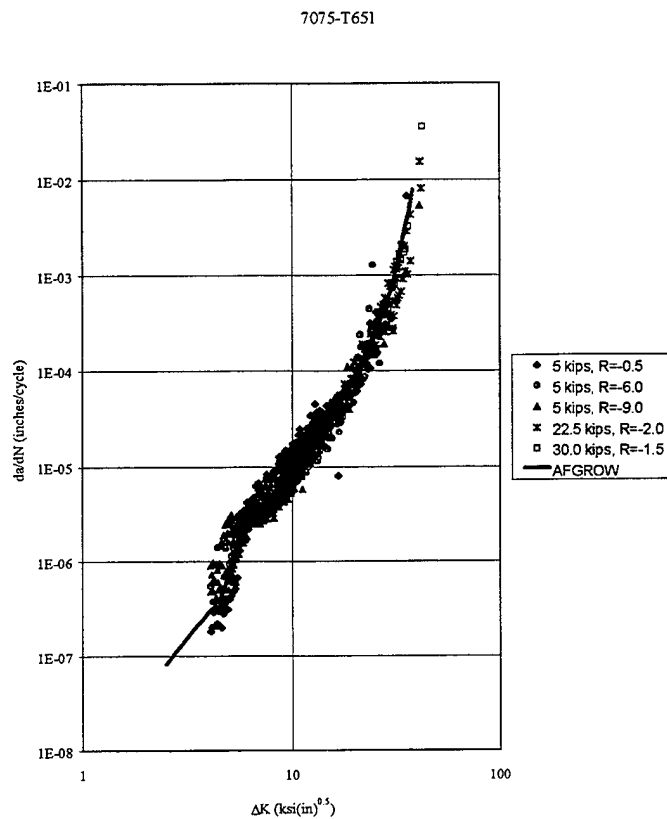


**Figure 11. Composite Fatigue Crack Growth Rate Plot for 7075-T651 Aluminum**

The solid line in Figure 11 is the AFGROW  $da/dN$  vs.  $\Delta K$  curve for  $R = -0.33$  (or any stress ratio less than  $-0.33$ ). While there was no statistical analysis performed in this study, the average fatigue crack growth rates were compared, to give cursory insight into the fatigue

crack growth trends. The average crack growth rates were compared at  $\Delta K$  values of 7, 10, and 13 ksi $\sqrt{\text{in}}$ , and are listed in Table 3.

**Table 3. Average Crack Growth Rates (in/cycle) at Several  $\Delta K$  Levels**

Stress Ratio, R	$\Delta K=7$ ksi $\sqrt{\text{in}}$	$\Delta K=10$ ksi $\sqrt{\text{in}}$	$\Delta K=13$ ksi $\sqrt{\text{in}}$
-0.5	4.7e-6	14e-6	27e-6
-6	4.0e-6	7.7e-6	18e-6
-9	3.1e-6	7.9e-6	20e-6

The values for R= -6 and -9 were similar, in that both of their values were less than those of R= -0.5. The shapes of the data curves for the three conditions in Figure 12, 13 and 14 also demonstrate this.

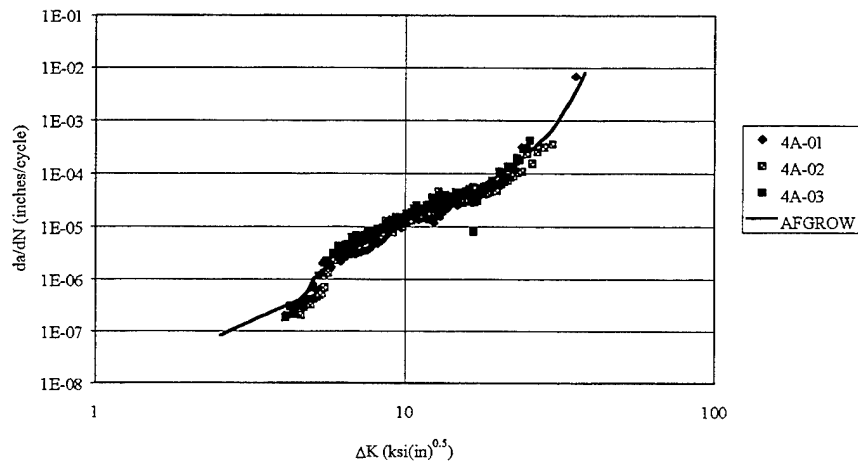


**Figure 12. Crack Growth Rate Plot for 7075-T651 Al with  $P_{\text{max}} = 5$  kips; R= -0.5**

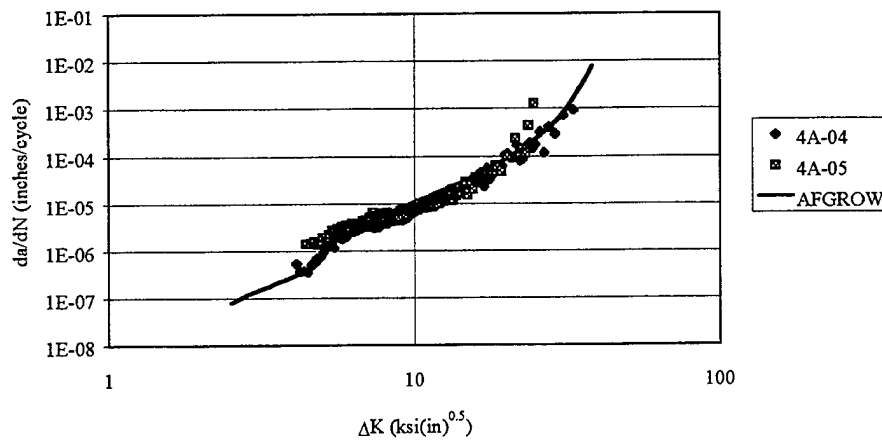


Figure 13. Crack Growth Rate Plot for 7075-T651 Al with  $P_{max} = 5$  kips;  $R = -6$

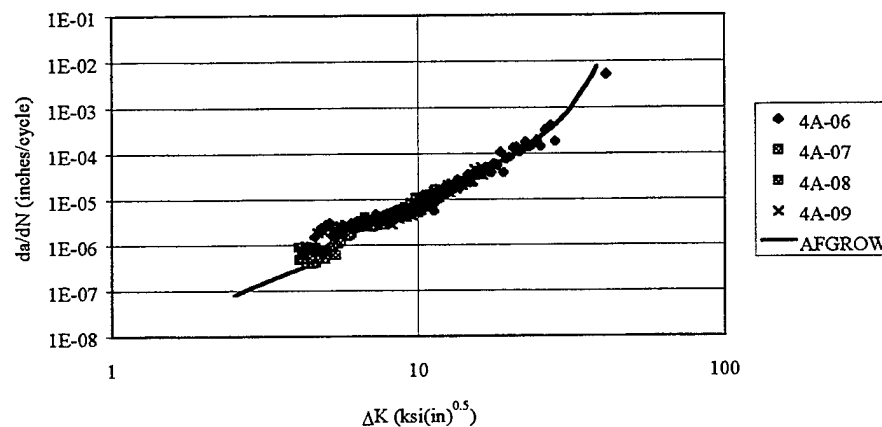


Figure 14. Crack Growth Rate Plot for 7075-T651 Al with  $P_{max} = 5$  kips;  $R = -9$

For  $R = -6$  and  $-9$  in Figures 13 and 14, respectively, the curves have a slight positive curvature, whereas Figure 12 for  $R = -0.5$  has an apparent, slight negative curvature. It is not conclusive whether the negative curvature is a real phenomena, as opposed to data scatter, or part of the lower (close to threshold) fatigue crack growth rate “double knees” reported in previous studies [15].

The AFGROW curve is the best fit of combined data. Even though five testing conditions were used, and keeping in mind the aforementioned discrepancies, the data in Figure 11 agrees with the AFGROW curve. The high end of  $\Delta K$  values fit good with the rest of the  $\Delta K$  values and the AFGROW curve. Due to the number of tests and various loading conditions, the data generated for this testing program is descriptive of most practical constant amplitude, compressive loading situations. The testing conditions and fatigue lifetimes for center-cracked panel testing is in Table 4. The  $da/dN$  vs.  $\Delta K$  data was used to modify the tabular data used in the AFGROW program. This data was then used to predict lifetimes of the surface cracked specimens.

**Table 4. Fatigue Lifetimes for 7075-T651 Al Under Reported Testing Conditions**

Specimen	Maximum load (kips)	Stress-Ratio ( R )	c, after pre- cracking (in)	Cycles to Failure
4A-01	5.0	-0.5	0.2390	423052
4A-02	5.0	-0.5	0.2010	666561
4A-03	5.0	-0.5	0.2050	480772
4A-04	5.0	-6.0	0.2010	449281
4A-05	5.0	-6.0	0.2325	232796
4A-06	5.0	-9.0	0.2070	285875
4A-07	5.0	-9.0	0.2005	484490
4A-08	5.0	-9.0	0.1995	388647
4A-09	5.0	-9.0	0.2030	302908
4A-11	22.5	-2.0	0.1930	1962
4A-12	22.5	-2.0	0.1910	2508
4A-13	30.0	-1.5	0.1935	455

One possible explanation of the scatter in the data is the fact that all testing was performed under laboratory conditions, where humidity levels were not held constant. Data from a recent in-house experimental effort [16] showed that 7075-T651 was effected by

differences in humidity levels. Generally, tests performed under high humidity conditions (>85%) showed a higher crack growth rate than data taken under low humidity conditions (<15%). Data for these two humidity level extremes was converted to the equivalent of  $R=-0.33$  using the Harter T-Method [17], and is shown for comparison with the test data taken for this effort in Figure 15.

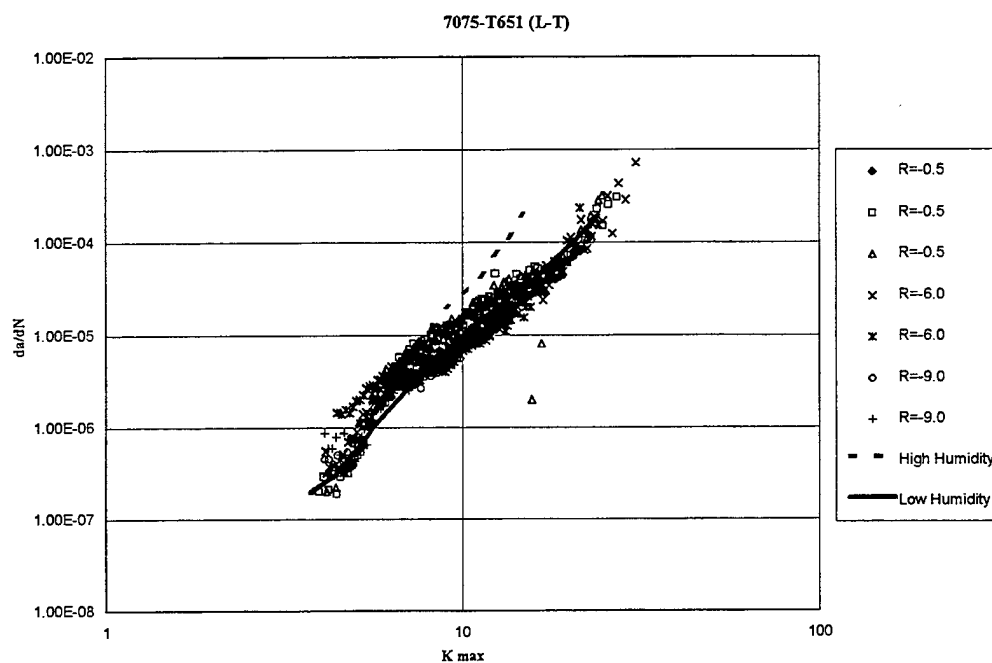


Figure 15. Composite Data Compared to High and Low Humidity Data for 7075-T651

It should be noted that the data used to generate the curves for rates above  $1.0\text{E-}05$  in/cycle were not plentiful. Similar data from other unpublished studies has indicated that the data for “wet” and “dry” environments tend to converge to higher crack growth rates. It is plausible that this could be explained by the time required for a humidity reaction to occur. However, if true, this would also be a function of loading frequency. In any event,



the data for these tests seems to fall within the band of the high and low humidity data, when adjusted to  $R=-0.33$ .

#### 4.1.2. 2024-T3 Aluminum Specimens

Four 2024-T3 center-cracked specimens were tested. The limited testing of 2024-T3 aluminum was reported, due to frequent buckling failures at the higher stress ratios. Several specimens buckled in the presence of anti-buckling guides. The  $da/dN$  vs.  $\Delta K$  data that was collected, can be seen in Figure 16, and plots for each specimen can be found in Figures 17 and 18.

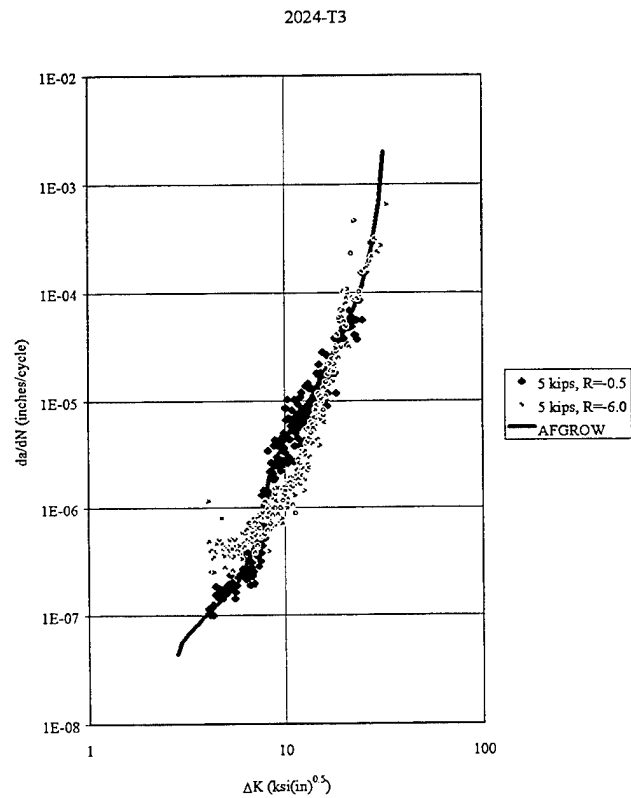
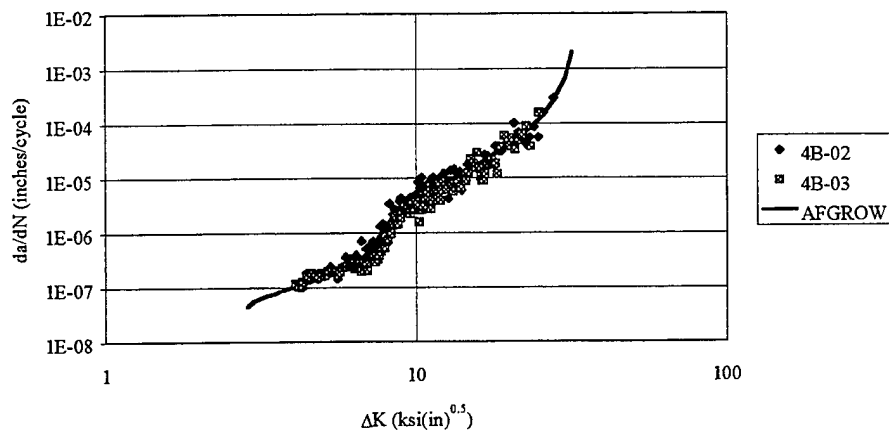
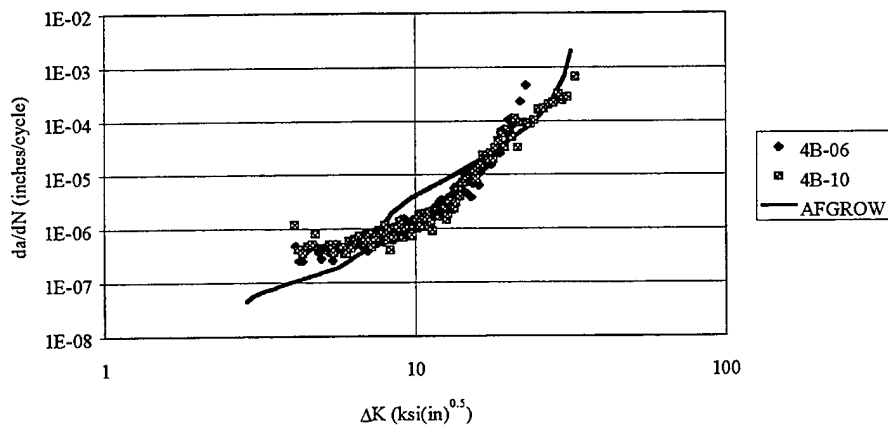


Figure 16. Composite Fatigue Crack Growth Rate Plot for 2024-T3 Aluminum



**Figure 17. Crack Growth Rate Plot for 2024-T3 Al with  $P_{max}$  = 5 kips;  $R$  = -0.5**



**Figure 18. Crack Growth Rate Plot for 2024-T3 Al with  $P_{max}$  = 5 kips;  $R$  = -6**

These curves have a distinct difference for the two different testing conditions. The curve for  $R=-6$ , Figure 18, has a positive curvature, and the curve for  $R=-0.5$ , Figure 17, has a negative curvature. These curves are consistent with the 7075 curves, but the  $R=-6$  curve does not have a “knee” at the lower end, like the other curves. The specimens with  $R= -6$

have a slower crack growth rate at the 10 ksi√in level, compared to  $R=-0.5$ . The 7075 aluminum behaves similarly. The testing conditions and fatigue lifetimes for center-cracked-panel tests are in Table 5.

**Table 5. Fatigue Lifetimes for 2024-T3 Al Under Reported Testing Conditions**

Specimen	Maximum load (kips)	R-ratio	c, after pre- cracking (in)	Cycles to Failure
4B-02	5.0	-0.5	0.1990	1753510
4B-03	5.0	-0.5	0.1995	2444381
4B-06	5.0	-6.0	0.2000	1458099
4B-10	5.0	-6.0	0.2015	1394955

Due to the limited number of 2024-T3 aluminum specimens tested under these conditions, it is not obvious if this data can be considered conclusive, especially, in the lower  $da/dN$  vs.  $\Delta K$  ranges. As the fatigue crack grows in finite width specimens, the net section stress elevates to values that induce large amounts of plasticity. It is possible that in the high stress ratio case ( $R= -6.0$ ), large amounts of plasticity may be influencing the fatigue crack growth rates beyond what is considered valid under linear elastic fracture mechanics. It is interesting to note that the fatigue crack growth rates for the high compressive stress ratios appear to be less than those at lesser negative stress ratios. This is contrary to earlier reports that higher negative stress ratio's would increase (accelerate) the fatigue crack growth rates in some aluminum alloys, especially 2024-T3 aluminum [5].

#### 4.2. Surface-Cracked Panel Testing

The surface-cracked specimens had a 0.10-inch EDM semi-circular notch machined in the center of the panel. The specimens were precracked by load shedding from 14 kips to 7.0 kips with  $R = -0.5$  and crack increments of 0.01 inch. The crack length at the beginning of the test was at least 0.05 inch beyond the notch to eliminate “stress history” effects. The half-crack lengths,  $c$ , were recorded at 0.005-inch increments, and the back of the panel was monitored to determine when the surface crack propagated through the panel thickness to become a through-thickness crack. Once the crack became a through-thickness crack, the half-crack lengths were recorded at 0.05-inch increments. The crack shape at break-through and cycles to break-through were compared to AFGROW predictions.

The life predictions in AFGROW are made with  $da/dN$  vs.  $\Delta K$  data generated using traditional Linear Elastic Fracture Methods (LEFM) methods, and engineering assumptions [17]. Since the loading in this study was constant amplitude, no “closure” models were used in AFGROW. However, when performing fatigue crack growth life predictions under spectrum loading conditions, engineers can incorporate these “closure” effects using the Wheeler [18], Willenborg [19], or Harter [20] crack growth retardation models. These various models take in to account the load history by estimating the amount of time it takes a crack to grow out of a plastic zone imposed by “overloads” or “underloads” in the fatigue spectrum.

#### 4.2.1. 7075-T651 Aluminum Specimens

Three specimens of 7075-T651 surface-cracked panels were tested. The fatigue crack growth lifetime for the surface-cracked panel can be broken down into the cycle count required for break-through, and the cycle count from break-through to failure. These two lifetimes were predicted with AFGROW, using tabular  $da/dN$  vs.  $\Delta K$  data, which included the results of center-cracked-panel testing. A semi-circular crack, corresponding to the crack length after precracking, was entered into AFGROW (center semi-elliptic configuration), and the predicted cycle count at break-through was recorded in Table 6. The half-crack length, predicted at break-through, was also recorded. The half-crack length at break-through was then entered into AFGROW (center-through-crack configuration) and the predicted cycle count to failure is reported in Table 7. The quarter-crack length was also entered into AFGROW for comparison.

Table 6. Fatigue and Crack Shape Data from Precracking to Break-Through

Specimen	Alloy	half crack length, $c$ (inches)			Surface crack lifetime (cycles)	
		after Pre-cracking	after breakthrough	AFGROW prediction	Testing	AFGROW
5A-01	7075-T6	0.1015	0.3040	0.344	362078	457871
5A-02	7075-T6	0.0915	0.3110	0.346	421277	543827
5A-03	7075-T6	0.0935	0.3315	0.345	390083	524844
5B-03	2024-T3	0.1600	0.1905	0.286	152015	65800
5B-04	2024-T3	0.0925	0.3155	0.304	764129	1708000

**Table 7. Fatigue Data from Break-Through to Failure for Different Initial Crack Lengths**

Specimen	Alloy	Through crack lifetime (cycles)		
		Testing	AFGROW* prediction	AFGROW** prediction
5A-01	7075-T6	189783	70902	146391
5A-02	7075-T6	140534	69284	141604
5A-03	7075-T6	104139	64808	131026
5B-03	2024-T3	807033	683969	1387191
5B-04	2024-T3	594786	238462	879497

\* Center-through-crack configuration with inputted initial crack length as listed in the fourth column in Table 6.

\*\* Center-through-crack configuration with inputted initial crack length as one-half the values in the fourth column in Table 6.

The results in Table 6 show that the predicted lifetimes from precracking to break-through (surface crack lifetime) were consistently nonconservative. The predicted lifetimes from break-through to failure were consistently conservative, and might be attributed to assumptions made in the AFGROW program. First, AFGROW assumes that a growing crack is either a surface crack or a through-crack during the course of the analysis. AFGROW does this by assuming that a part-through crack converts to a through-crack at approximately 90% of the specimen thickness. However, at break-through, the crack on the backside of the specimen had a shorter length than on the front side where the measurements were taken. Secondly, the part-through crack stress intensity solution in AFGROW is based on the earlier work of Newman and Raju [21], and was not fully implemented for these analyses. More complete stress intensity solutions for this part-through-crack case can be found in the literature [21,22], and are presently being incorporated into the AFGROW code.

In this study, the specimen backside was not monitored after break-through, and since it was assumed that the surface crack transforms into a through-crack in a negligible amount of cycles, could have been a source of error. It may be more realistic to use an “effective” crack length, which is not as long as the “measured” crack length, for the purpose of fatigue crack growth rate analysis. This approach was implemented in this study. It can be seen that if the “break-through” half-crack length values, inputted into AFGROW, are scaled by 0.5 inch, then the accuracy of the three AFGROW predictions increases.

#### **4.2.2. 2024-T3 Aluminum Specimens**

Two specimens of 2024-T3 surface-cracked panels were tested. The results were compared to AFGROW in Table 6. The discrepancy for panel 5B-03 can be explained from the precracking schedule. The crack arrested during precracking and the panel was cycled for over 2 million cycles. Although the crack was not growing on the surface, it most likely was growing in the thickness direction. Once the precracking was finished, the aspect ratio of the crack was much larger than it would have been, had the crack not arrested on the surface. It is believed that the large aspect ratio resulted in a quicker breakthrough when the testing began.

#### **4.2.3. Additional Testing**

Due to the limited amount of test cases performed for the 2024-T3 aluminum and the availability of additional 7075-T651 specimens, two additional test cases were run at different maximum stresses and stress ratios for the 7075-T651 aluminum material. This testing was performed in order to investigate the effect of higher maximum stresses for this material. These tests were included to address whether the crack growth rate behavior under negative R conditions is drastically effected when the maximum stresses applied are above 20-30% of yield stress.



The load conditions were chosen to allow a maximum compressive load of -45 kips. This level of compression was equal to that used for the test shown in Table 3 for this alloy ( $R = -9.0$ ). Due to the high operating stresses used in these two cases, limited “upper end”  $da/dN$  vs.  $\Delta K$  data was gathered.

The first case was for a maximum load of 22.5 kips (~40% of yield stress) with a stress ratio of -2.0. The fatigue crack growth rates compared well with those implemented in AFGROW, and the plot is shown in Figure 19.

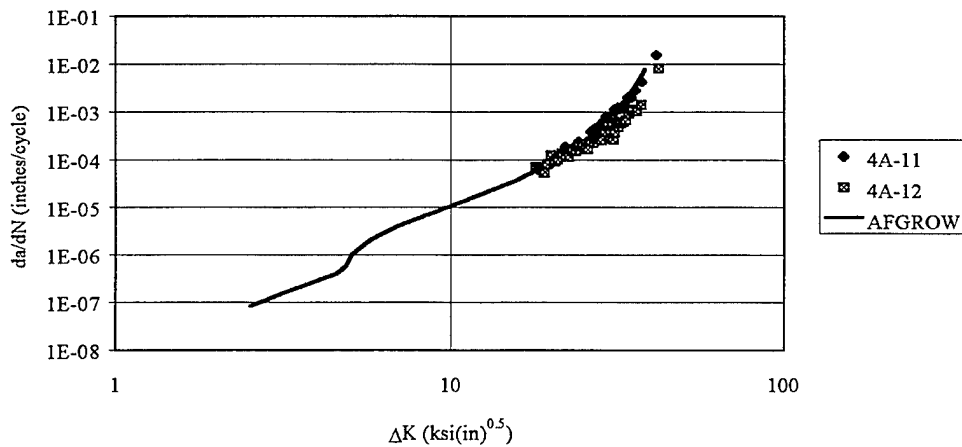


**Figure 19. Crack Growth Rate Plot for 7075-T651 Al with  $P_{max} = 22.5$  kips;  $R = -2$**

The second case was for a maximum load of 30 kips (>50% of yield stress) with a stress ratio of -1.5. The fatigue crack growth rates compared well with those implemented in AFGROW, and the plot is shown in Figure 20.

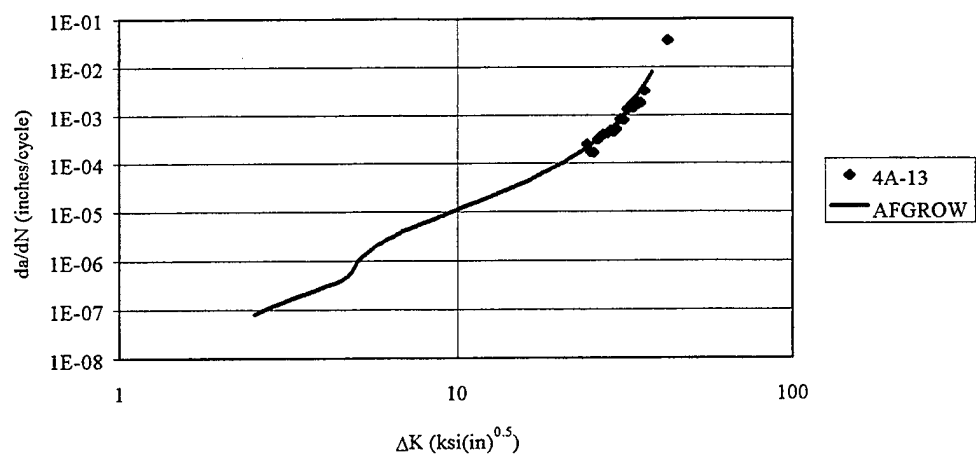


Figure 20. Crack Growth Rate Plot of 7075-T651 Al with  $P_{max} = 30$  kips;  $R = -1.5$

## 5. REFERENCES

- [1] Krishnan, S., Boyd, K.L., Harter, J.A. "AFGROW User's Manual: Version 3.0.4," *WL-TM-96-3096*, Air Force Flight Dynamics Directorate, Wright-Patterson Air Force Base, OH, July 1995.
- [2] Walker, K. "The Effect of Stress Ratio During Crack Propagation and Fatigue for 2024-T3 and 7075-T6 Aluminum" Effects of Environment and Complex Load History on Fatigue Life, *ASTM STP 462*, American Society for Testing and Materials, 1970, pp. 1-14.
- [3] Forman, V.E. Kearney, R.M. Engle, "Numerical Analysis of Crack Propagation in Cyclic-Loaded Structures," Journal of Basic Engineering, *Transactions of the ASME*, September 1967, pp. 459-464.
- [4] Illg, W., McEvily, A.J., Jr., "The Rate of Fatigue-Crack Propagation for Two Aluminum Alloys Under Completely Reversed Loading", *NASA TN-D-52*, National Aeronautics and Space Administration, July, 1959.
- [5] Hudson, M., "Effect of Stress Ratio on Fatigue-Crack Growth in 7075-T6 and 2024-T3 Aluminum-Alloy Specimens" *NASA TN-D-5390*, National Aeronautics and Space Administration, August 1969.
- [6] M.T. Yu, T.H. Topper, P.A., "The Effects of Stress Ratio, Compressive Load and Underload on the Threshold Behavior of a 2024-T351 Aluminum Alloy", *Fatigue 84*, Engineering Materials Advisory Services Ltd., c1984, pp. 179-190.
- [7] Elber, W., "The Significance of Fatigue Crack Closure", Damage Tolerance in Aircraft Structures, *ASTM STP 486*, American Society for Testing and Materials., 1971, pp. 230-242.
- [8] Newman, J.C., Jr., "Finite Element Analysis of Fatigue Crack Propagation-Including the Effects of Crack Closure," *Ph. D. Thesis*, Virginia Polytechnic Institute and State University, Blacksburg, Va., May 1974.
- [9] Zienkiewicz, O.C., Valliappan, S., and King I.P., "Elasto-Plastic Solutions of Engineering Problems 'Initial Stress', Finite Element Approach," *International Journal for Numerical Methods in Engineering*, Vol. I., 1968, pp. 75-100.
- [10] Newman, J.C., Jr., "A Finite-Element Analysis of Fatigue Crack Closure," Mechanics of Crack Growth, *ASTM STP 590*, American Society for Testing and Materials, 1976, pp. 281-301.

- [11] Newman, J.C., Dawicke, D.S., Sutton, M.A., and Bigelow, C.A., "A Fracture Criterion for Widespread Cracking in Thin Sheet Aluminum Alloys," International Committee on Aeronautical Fatigue, 17<sup>th</sup> Symposium, Durability and Structural Integrity of Airframes, Stockholm, Sweden, 1993, pp. 443-467.
- [12] Newman, J.C., "Fracture Analysis of Stiffened Panels Under Biaxial Loading with Widespread Cracking," *NASA TM-110197*, NASA Langley Research Center, October 1995.
- [13] Newman, J.C., Jr., "Finite-Element Analysis of Crack Growth Under Monotonic and Cyclic Loading," *ASTM-STP 637*, American Society for Testing and Materials, 1977, pp. 56-80.
- [14] Newman, J.C., Jr., "An Elastic-Plastic Finite Element Analysis of Crack Initiation, Stable Crack Growth, and Instability," *Fracture Mechanics: Fifteenth Symposium, ASTM STP 833*, American Society for Testing and Materials, 1984, pp. 93-117.
- [15] Boyd, K.L., Jansen, D.A., Krishnan, S., Harter, J.A., "Structural Analysis and Verification of Aircraft Structures, Vol. I. Characterization of 7075-T7351 Aluminum; MODGRO Verification; MODGRO GUI Development," *WL-TR-95-3090*, Air Force Flight Dynamics Directorate, Wright-Patterson Air Force Base, OH, January 1996.
- [16] Jansen, D.A., Boyd, K.L., "Structural Integrity and Verification of Aircraft Structures- Vol. 5: Verification of Humidity and Age Effects on C/KC-135 Aircraft Fuselage Skin Alloys 2024-T3, 2024-T4 and 7075-T6," *WL-TR-95-3104*, Flight Dynamics Directorate, Wright-Patterson AFB, Ohio, August 1996.
- [17] Harter, J. A., "MODGRO User's Manual-Version 1.2," *AFWAL-TM-88-157-FIBE*, Air Force Flight Dynamics Laboratory, Wright-Patterson Air Force Base, OH, February 1988 (Revised July 1994).
- [18] Wheeler, O.J., "Spectrum Loading and Crack Growth," Transactions, American Society of Mechanical Engineering, *Journal of Basic Engineering*, 94, 1972, pp. 181-186.
- [19] Willenborg, J.D., Engle, R.M., and H. A. Wood, "A Crack Growth Retardation Model Using an Effective Stress Concept," *AFFDL-TM-71-1-FBR*, Air Force Flight Dynamics Laboratory, 1970.
- [20] Harter, J.A., "AFGROW- Formerly MODGRO," Interagency Working Group for NASGRO Development, Second Meeting Summary, August 1995.

- [21] Newman, J.C., Jr., Raju, I.S., "Stress Intensity Factor Equations for Cracks in Three Dimensional Finite Bodies Subjected to Tension and Bending Loads," *NASA-TM-85793*, NASA Langley Research Center, 1984.
- [22] Bates, P.R., "MH-53J Stress Intensity Factor Models and Solutions," *Final Technical Report, GTRI Project A-9311*, Georgia Institute of Technology, March 1994.

## APPENDIX A

**Figure A.1: Detailed Information for Specimen Tests**

7075-T651 - Center Notch							
Specimen	Mach	Rpre	P(kips)	Rtest	Pre	Test	End
4A-01	10	-0.5	5.0	-0.5	3-27	3-29	**
4A-02	4	-0.5	5.0	-0.5	5-9	7-18	8-10
4A-03	10	-0.5	5.0	-0.5	5-8	7-21	8-10
4A-04	4	-0.5	5.0	-6.0	5-12	5-19	6-20
4A-05	3	-0.5	5.0	-6.0	5-15	7-21	8-10
4A-06	4	-0.5	5.0	-9.0	5-16	8-15	9-20
4A-07	4	-0.5	5.0	-9.0	5-17	**	6-27
4A-08	4	-0.5	5.0	-9.0	5-18	6-27	7-14
4A-09	3	-0.5	5.0	-9.0	5-18	8-15	9-18
4A-11	3	-0.5	22.5	-2.0	11-8	11-8	11-9
4A-12	4	-0.5	22.5	-2.0	11-8	11-14	11-14
4A-13	3	-0.5	30.0	-1.5	11-14	11-15	11-15
2024-T3 - Center Notch							
Specimen	Mach	Rpre	P(kips)	Rtest	Pre	Test	End
4B-02	10	-0.5	5.0	-0.5	**	8-21	10-5
4B-03	10	-0.5	5.0	-0.5	4-26	10-5	10-19
4B-06	3	-0.5	5.0	-6.0	4-26	9-22	10-11
4B-10	4	-0.5	5.0	-6.0	5-9	9-22	10-11
7075-T651 - Surface Flaw							

Specimen	Mach	Rpre	P(kips)	Rtest	Pre	Test	End
5A-01	10-3	-0.5	7.0	-4.0	10-19	11-1	11-7
5A-02	3	-0.5	7.0	-4.0	10-23	10-24	10-27
5A-03	3	-0.5	7.0	-4.0	10-27	10-30	11-1

2024-T3 - Surface Flaw							
Specimen	Mach	Rpre	P(kips)	Rtest	Pre	Test	End
5B-03	12-3	-0.5	7.0	-4.0	7-10	10-16	10-20
5B-04	4	-0.5	7.0	-4.0	10-18	10-20	10-31